Large-area fabrication of TiN nanoantenna arrays for refractory plasmonics in the mid-infrared by femtosecond direct laser writing and interference lithography [Invited]

Shahin Bagheri,[1] Christine M. Zgrabik,[2] Timo Gissibl,[1] Andreas Tittl,[1] Florian Sterl,[1] Ramon Walter,[1] Stefano De Zuani,[3] Audrey Berrier,[3] Thomas Stauden,[4] Gunther Richter,[5] Evelyn L. Hu,[2] and Harald Giessen[1*]

[1]*4th Physics Institute and Research Center SCoPE, University of Stuttgart, Pfaffenwaldring 57, Stuttgart, Germany*
[2]*School of Engineering and Applied Sciences, Harvard University, Cambridge, MA 02138, USA*
[3]*1st Physics Institute and Research Center SCoPE, University of Stuttgart, Pfaffenwaldring 57, Stuttgart, Germany*
[4]*Fachgebiet Nanotechnologie, Technische Universität Ilmenau, Ilmenau, Germany*
[5]*Max-Planck-Institut für Intelligente Systeme, D-70569 Stuttgart, Germany*
[*]*h.giessen@pi4.uni-stuttgart.de*

Abstract: Robust plasmonic nanoantennas at mid-infrared wavelengths are essential components for a variety of nanophotonic applications ranging from thermography to energy conversion. Titanium nitride (TiN) is a promising candidate for such cases due to its high thermal stability and metallic character. Here, we employ direct laser writing as well as interference lithography to fabricate large-area nanoantenna arrays of TiN on sapphire and silicon substrates. Our lithographic tools allow for fast and homogeneous preparation of nanoantenna geometries on a polymer layer, which is then selectively transferred to TiN by subsequent argon ion beam etching followed by a chemical wet etching process. The antennas are protected by an additional Al_2O_3 layer which allows for high-temperature annealing in argon flow without loss of the plasmonic properties. Tailoring of the TiN antenna geometry enables precise tuning of the plasmon resonances from the near to the mid-infrared spectral range. Due to the advantageous properties of TiN combined with our versatile large-area and low-cost fabrication process, such refractory nanoantennas will enable a multitude of high-temperature plasmonic applications such as thermophotovoltaics in the future.

OCIS codes: (250.5403) Plasmonics; (220.4241) Nanostructure fabrication; (160.3918) Metamaterial.

References and links

1. M. Tame, K. McEnery, Ş. Özdemir, J. Lee, S. Maier, and M. Kim, "Quantum plasmonics," Nat. Phys. **9**(6), 329–340 (2013).
2. S. Berweger, J. M. Atkin, R. L. Olmon, and M. B. Raschke, "Light on the tip of a needle: Plasmonic nanofocusing for spectroscopy on the nanoscale," J. Phys. Chem. Lett. **3**(7), 945–952 (2012).
3. N. Liu, M. L. Tang, M. Hentschel, H. Giessen, and A. P. Alivisatos, "Nanoantenna-enhanced gas sensing in a single tailored nanofocus," Nat. Mater. **10**(8), 631–636 (2011).
4. N. Li, A. Tittl, S. Yue, H. Giessen, C. Song, B. Ding, and N. Liu, "DNA-assembled bimetallic plasmonic nanosensors," Light Sci. Appl. **3**(12), e226 (2014).
5. G. Dolling, M. Wegener, C. M. Soukoulis, and S. Linden, "Negative-index metamaterial at 780 nm wavelength," Opt. Lett. **32**(1), 53–55 (2007).
6. N. Liu, M. Mesch, T. Weiss, M. Hentschel, and H. Giessen, "Infrared perfect absorber and its application as plasmonic sensor," Nano Lett. **10**(7), 2342–2348 (2010).
7. A. Tittl, P. Mai, R. Taubert, D. Dregely, N. Liu, and H. Giessen, "Palladium-based plasmonic perfect absorber in the visible wavelength range and its application to hydrogen sensing," Nano Lett. **11**(10), 4366–4369 (2011).
8. K. Chen, R. Adato, and H. Altug, "Dual-band perfect absorber for multispectral plasmon-enhanced infrared spectroscopy," ACS Nano **6**(9), 7998–8006 (2012).

#246613 Received 23 Jul 2015; revised 20 Sep 2015; accepted 14 Oct 2015; published 22 Oct 2015

Corrected: 24 November 2015

9. R. Walter, A. Tittl, A. Berrier, F. Sterl, T. Weiss, and H. Giessen, "Large-Area low-cost tunable plasmonic perfect absorber in the near-infrared by colloidal etching lithography," Adv. Opt. Mater. **3**(3), 398–403 (2015).
10. N. Liu, L. Langguth, T. Weiss, J. Kästel, M. Fleischhauer, T. Pfau, and H. Giessen, "Plasmonic analogue of electromagnetically induced transparency at the Drude damping limit," Nat. Mater. **8**(9), 758–762 (2009).
11. C. Wu, A. B. Khanikaev, R. Adato, N. Arju, A. A. Yanik, H. Altug, and G. Shvets, "Fano-resonant asymmetric metamaterials for ultrasensitive spectroscopy and identification of molecular monolayers," Nat. Mater. **11**(1), 69–75 (2011).
12. D. Lin, P. Fan, E. Hasman, and M. L. Brongersma, "Dielectric gradient metasurface optical elements," Science **345**(6194), 298–302 (2014).
13. G. Naik, J. Kim, and A. Boltasseva, "Oxides and nitrides as alternative plasmonic materials in the optical range," Opt. Mater. Express **1**(6), 1090–1099 (2011).
14. K. Appavoo, D. Y. Lei, Y. Sonnefraud, B. Wang, S. T. Pantelides, S. A. Maier, and R. F. Haglund, Jr., "Role of defects in the phase transition of VO_2 nanoparticles probed by plasmon resonance spectroscopy," Nano Lett. **12**(2), 780–786 (2012).
15. B. Gholipour, J. Zhang, K. F. MacDonald, D. W. Hewak, and N. I. Zheludev, "An all-optical, non-volatile, bidirectional, phase-change meta-switch," Adv. Mater. **25**(22), 3050–3054 (2013).
16. N. Strohfeldt, A. Tittl, M. Schäferling, F. Neubrech, U. Kreibig, R. Griessen, and H. Giessen, "Yttrium hydride nanoantennas for active plasmonics," Nano Lett. **14**(3), 1140–1147 (2014).
17. F. Sterl, N. Strohfeldt, R. Walter, R. Griessen, A. Tittl, and H. Giessen, "Magnesium as novel material for active plasmonics in the visible wavelength range," Nano Lett. (2015), doi:10.1021/acs.nanolett.5b03029.
18. U. Guler, A. Boltasseva, and V. M. Shalaev, "Refractory plasmonics," Science **344**(6181), 263–264 (2014).
19. S. Fan, "Photovoltaics: An alternative 'Sun' for solar cells," Nat. Nanotechnol. **9**(2), 92–93 (2014).
20. W. Li, U. Guler, N. Kinsey, G. V. Naik, A. Boltasseva, J. Guan, V. M. Shalaev, and A. V. Kildishev, "Refractory plasmonics with titanium nitride: broadband metamaterial absorber," Adv. Mater. **26**(47), 7959–7965 (2014).
21. M. Diem, T. Koschny, and C. M. Soukoulis, "Wide-angle perfect absorber/thermal emitter in the terahertz regime," Phys. Rev. B **79**(3), 033101 (2009).
22. E. Rousseau, A. Siria, G. Jourdan, S. Volz, F. Comin, J. Chevrier, and J. J. Greffet, "Radiative heat transfer at the nanoscale," Nat. Photonics **3**(9), 514–517 (2009).
23. C. Maus, T. Stauden, G. Ecke, K. Tonisch, and J. Pezoldt, "Smooth ceramic titanium nitride contacts on AlGaN/GaN-heterostructures," Semicond. Sci. Technol. **27**(11), 3264–3294 (2012).
24. G. V. Naik, V. M. Shalaev, and A. Boltasseva, "Alternative plasmonic materials: Beyond gold and silver," Adv. Mater. **25**(24), 3264–3294 (2013).
25. U. Guler, V. M. Shalaev, and A. Boltasseva, "Nanoparticle plasmonics: going practical with transition metal nitrides," Mater. Today **18**(4), 227–237 (2015).
26. U. Guler, J. C. Ndukaife, G. V. Naik, A. G. A. Nnanna, A. V. Kildishev, V. M. Shalaev, and A. Boltasseva, "Local heating with lithographically fabricated plasmonic titanium nitride nanoparticles," Nano Lett. **13**(12), 6078–6083 (2013).
27. S. Bagheri, K. Weber, T. Gissibl, T. Weiss, F. Neubrech, and H. Giessen, "Fabrication of square-centimeter plasmonic nanoantenna arrays by femtosecond direct laser writing lithography: effects of collective excitations on SEIRA enhancement," ACS Photonics **2**(6), 779–786 (2015).
28. S. Bagheri, H. Giessen, and F. Neubrech, "Large-area antenna-assisted SEIRA substrates by laser interference lithography," Adv. Opt. Mater. **2**(11), 1050–1056 (2014).
29. G. V. Naik, B. Saha, J. Liu, S. M. Saber, E. A. Stach, J. M. K. Irudayaraj, T. D. Sands, V. M. Shalaev, and A. Boltasseva, "Epitaxial superlattices with titanium nitride as a plasmonic component for optical hyperbolic metamaterials," Proc. Natl. Acad. Sci. U.S.A. **111**(21), 7546–7551 (2014).
30. G. V. Naik, J. L. Schroeder, X. Ni, A. V. Kildishev, T. D. Sands, and A. Boltasseva, "Titanium nitride as a plasmonic material for visible and near-infrared wavelengths," Opt. Mater. Express **2**(4), 478–489 (2012).
31. T. Weiss, G. Granet, N. A. Gippius, S. G. Tikhodeev, and H. Giessen, "Matched coordinates and adaptive spatial resolution in the Fourier modal method," Opt. Express **17**(10), 8051–8061 (2009).
32. A. Mitsuo, S. Uchida, N. Nihira, and M. Iwaki, "Improvement of high temperature oxidation resistance of titanium nitride and titanium carbide films by aluminum ion implantation," Surf. Coat. Tech. **103–104**, 98–103 (1998).
33. U. Guler, A. V. Kildishev, A. Boltasseva, and V. M. Shalaev, "Plasmonics on the slope of enlightenment: the role of transition metal nitrides," Faraday Discuss. **178**, 71–86 (2015).
34. S. T. Sundari, R. Ramaseshan, F. Jose, S. Dash, and A. K. Tyagi, "Investigation of temperature dependent dielectric constant of a sputtered TiN thin film by spectroscopic ellipsometry," J. Appl. Phys. **115**(3), 033516 (2014).
35. A. Tittl, A. K. Michel, M. Schäferling, X. Yin, B. Gholipour, L. Cui, M. Wuttig, T. Taubner, F. Neubrech, and H. Giessen, "A Switchable Mid-Infrared Plasmonic Perfect Absorber with Multispectral Thermal Imaging Capability," Adv. Mater. **27**(31), 4597–4603 (2015).

1. Introduction

Plasmonics is at the heart of many aspects of nano-optics and photonics, where it has been utilized for a broad variety of research and commercial applications. One significant feature of plasmonic resonators is their ability to concentrate light into deep subwavelength volumes, enabling efficient light confinement on the nanoscale as well as antenna-enhanced sensing

#246613 Received 23 Jul 2015; revised 20 Sep 2015; accepted 14 Oct 2015; published 22 Oct 2015

approaches [1–4]. Building on this concept, plasmonic geometries have led to the realization of artificial optical materials with novel properties such as negative refraction [5], perfect absorption [6–9], and the plasmonic analogue of electrically induced transparency from atomic physics [10,11]. Plasmonic geometries commonly rely on noble metals such as gold (Au), silver (Ag) and aluminum (Al) due to their comparatively small Ohmic losses and well-understood optical and mechanical properties.

However, in order to improve the efficiency of current plasmonic designs and to realize novel concepts, there is an increased need for additional classes of plasmonic materials. Particularly, semiconductor materials such as highly doped silicon (Si) [12] and transparent conducting oxides (TCO) [13] have been introduced due to their tunable optical properties and compatibility with standard industrial chip-scale processing (CMOS) technologies. Furthermore, materials which undergo a phase change in response to an external stimulus such as vanadium dioxide (VO_2) [14], germanium antimony telluride (GST) [15], yttrium (Y) [16] and magnesium [17] have been employed to realize active plasmonic devices.

Another crucial material-related challenge is the stability of plasmonic structures at the very high temperatures that are relevant to many industrial processes. This requirement is difficult to satisfy using metals with comparatively low melting points, and hence necessitates a transition to more stable, so-called refractory materials [18]. Such materials are chemically stable at temperatures above 2000°C and are thus ideal candidates for high-temperature plasmonic applications such as thermophotovoltaics [19], perfect absorption and thermal emission [20–22], and nanoscale-heat transfer systems [22]. This is especially important when operating plasmonic structures as thermal emitters, where high device temperatures are needed to achieve the desired emission wavelengths, e.g., in the mid- and near-infrared.

Titanium nitride (TiN) has emerged as a promising material for refractory plasmonics [18] and other high-temperature applications [23] due to its negative real value of permittivity and low interband loss in the near- and mid-infrared spectral range [24–26]. However, the fabrication of TiN nanostructures with tunable plasmonic resonances over large areas has proven challenging. In this work, we utilize fast and wafer-scale fabrication methods such as direct laser writing (DLW) [27] and laser interference lithography (LIL) [28] to create a regular polymer pattern, which is then selectively transferred into a TiN layer through a combination of dry and chemical wet etching processes. Following this approach, we achieve large-area nanoantenna arrays of TiN with tunable plasmon resonances from the near- to the mid-infrared spectral range. Due to the refractory properties of TiN, the fabricated nanoantennas are good candidates for high-temperature plasmonic applications, particularly when covered with an oxide-resistant layer with high-temperature stability such as Al_2O_3 or Si_3N_4.

2. TiN nanoantennas

A schematic drawing of the TiN nanoantenna fabrication process is shown in Fig. 1. First, substrates are sonicated for 10 minutes in acetone as well as isopropanol. In addition, the Si substrates undergo a 30 second hydrofluoric acid (49%) dip prior to sonication. Subsequently, the substrates are loaded into the sputtering chamber (AJA International ATC 2200-V6) and cleaned under vacuum condition by Ar plasma (25W). Afterwards a 50 nm TiN layer is deposited using non-reactive sputtering (10^{-8} Torr, RF power: 150 W, Ar flow: 40 sccm, deposition pressure: 4 mT, temperature: 20 C, applied bias: 100 V). Then, a 5 nm chromium (Cr) adhesion layer and a 100 nm gold (Au) intermediate layer are evaporated (Pfeiffer Vacuum Model PLS-500, 10^{-7} mbar). The purpose of the gold layer is to assist in the wet etching process as an additional mask since the polymer layer is partly damaged during the wet etching.

Figures 1(a)-1(f) show the fabrication processes of the nanoantennas. The photoresist (Nanoscribe IP-Dip, development in Microresist mr-dev 600 for 15 minutes) is drop-cast onto the multi-layer sample, and direct laser writing (Photonic Professional GT, Nanoscribe GmbH, Germany) is utilized to create nanoantenna patterns in the polymer. These patterns are then transferred first to the gold film via argon ion beam etching (Technics Plasma Model

#246613 Received 23 Jul 2015; revised 20 Sep 2015; accepted 14 Oct 2015; published 22 Oct 2015

R.I.B.-Etch 160, etching rate: 0.5 nm/sec) and then to the TiN film via a chemical wet etching process by using NH_4OH: H_2O_2: H_2O (1: 2: 5) solution (75°C, etching rate: 0.5 nm/sec). Afterwards, the sample is immersed in distilled water for 60 seconds and dried using nitrogen. Finally the photoresist and the gold layer are removed via oxygen plasma (Diener electronic Plasma-Surface-Technology, 100 min, 1.3 mbar, 160 W) and argon ion beam etching, respectively. Relative transmittance spectra of our nanoantenna arrays (200 × 200 μm^2) are measured using a Bruker Hyperion microscope coupled to a Bruker Vertex 80 spectrometer.

The proposed refractory plasmonic TiN nanoantenna design can be implemented using other large-area fabrication methods such as interference lithography. However, this requires optimization of photoresists and metal thicknesses as we demonstrate in the following. For manufacturing TiN nanoantenna arrays by interference lithography, the photoresist (ma-N 405) is spin-coated on Cr (2 nm) and Au (35 nm) layers and the development process is carried out in AZ826 developer for 48 seconds.

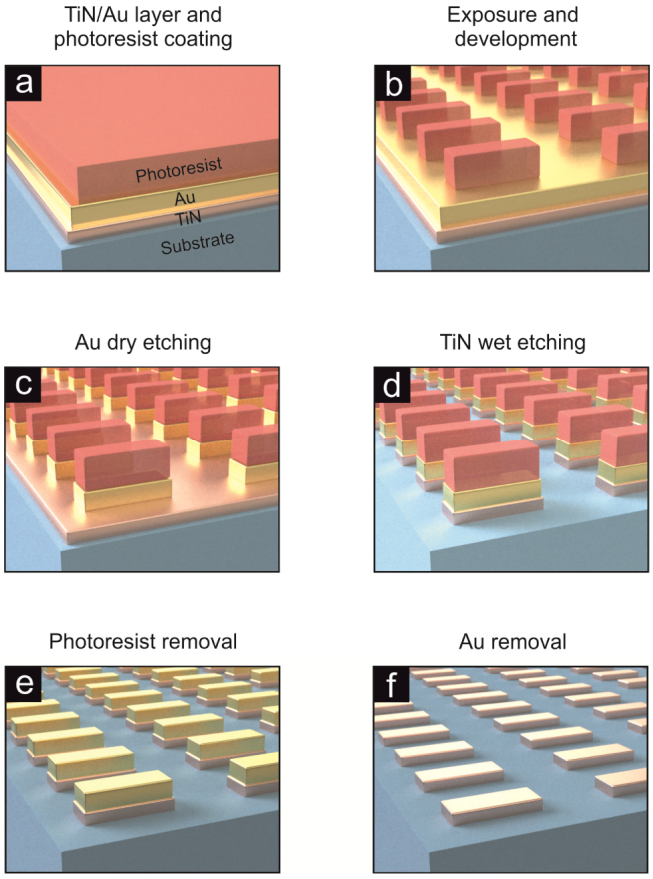

Fig. 1. Schematic drawing of the fabrication process of TiN nanoantennas: (a) 50 nm thick TiN films are sputtered and 100 nm thick Au films are evaporated on a substrate. Subsequently, the photoresist is coated on top. (b) Exposure and development processes create the antennas mask in the polymer, which is transferred first to (c) Au via argon ion beam dry etching and then to (d) the TiN film by chemical wet etching. (e) The photoresist and (f) gold are removed by oxygen plasma and argon ion beams, respectively. Additionally, an oxidation-resistant layer can be deposited onto the TiN antennas to protect them from oxygen when annealing at high temperatures.

#246613 Received 23 Jul 2015; revised 20 Sep 2015; accepted 14 Oct 2015; published 22 Oct 2015

3. Results and discussion

The fabricated nanoantennas provide a plasmon resonance which is strongly dependent on the antenna material and consequently the dielectric function of the TiN film. To investigate this further, we measure the dielectric function of the TiN films used in our fabrication process (thickness 50 nm) via spectroscopic ellipsometry (Woollam variable angle spectroscopic ellipsometer (VASE), spectral range 0.3 to 2.2 μm, angles of incidence varied from 45° to 65° in steps of 5°). The ellipsometric data are modeled by a general oscillator layer model with a mean square error (MSE) of 0.7. The real and imaginary parts of the dielectric function were extrapolated from the model up to the mid-infrared range as shown in Fig. 2(a) and 2(b) respectively. The real (ε_1) and the imaginary (ε_2) parts of the dielectric function of the TiN film on both silicon and sapphire substrates exhibit metallic behavior (negative real permittivity and low interband loss) in the near- and mid-infrared spectral regions, comparable to TiN films demonstrated by other groups [29]. The slight difference between dielectric functions of TiN film on silicon and sapphire substrate is to be expected since the different lattice matching of the substrates influences the dielectric functions of TiN films as demonstrated previously [30]. However, the modeled results show some sensitivity to the film thickness; therefore, we have verified the rate-estimated sputtering thickness by performing both Dektak profilometry and X-ray reflectometry measurements. We use these optical constants to estimate the plasmonic resonance of our nanoantennas by employing a Fourier modal method numerical simulation approach [31]. As expected, the geometry of the TiN nanoantennas plays an important role for tailoring the plasmon resonance wavelength over the near- and mid-infrared range. Figure 2(c) shows simulated relative transmittance spectra (parallel polarization) of the nanoantennas with different periodicities (P) and antenna lengths (L) on a sapphire substrate, demonstrating geometrical plasmon resonance tunability from the near- to mid-infrared (red: P = 1.5 μm and L = 1.0 μm, green: P = 2.0 μm and L = 1.5 μm, blue: P = 2.5 μm and L = 2.0 μm).

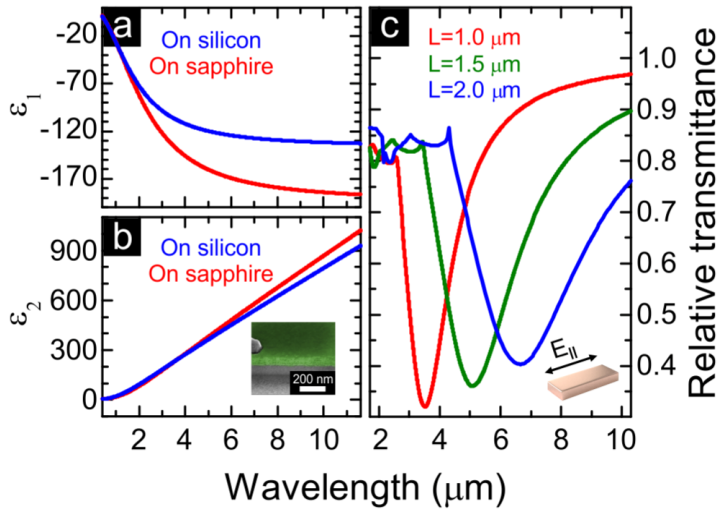

Fig. 2. (a) Real (ε_1) and (b) the imaginary (ε_2) parts of the dielectric function of the 50 nm thick TiN films on silicon (blue line) and sapphire (red line) substrates extracted from the modeled spectroscopic ellipsometry measurements and extrapolated to 12 μm. (c) The measured optical properties of the TiN film are used to simulate the plasmon resonance (polarization of the electric field $E_{\parallel}$ is parallel to the antenna long axis) of nanoantennas with different lengths (L) using a Fourier modal method numerical simulation, resulting in tunable plasmon resonances from near- to mid-infrared in spectral range. The kinks in the simulated plasmonic resonances (panel c) are Rayleigh anomalies due to grating resonances. A cross section SEM image of the TiN film is shown as the inset in Fig. 2(b).

#246613 Received 23 Jul 2015; revised 20 Sep 2015; accepted 14 Oct 2015; published 22 Oct 2015

Figure 3 shows the plasmon resonance of such a nanoantenna array (P = 1.5 μm, L = 0.83 μm), demonstrating good agreement between simulation and experiment. However, the slight difference between the simulation and the experiment could arise from the chemical wet etching process which causes imperfect walls and surface roughness of the antennas.

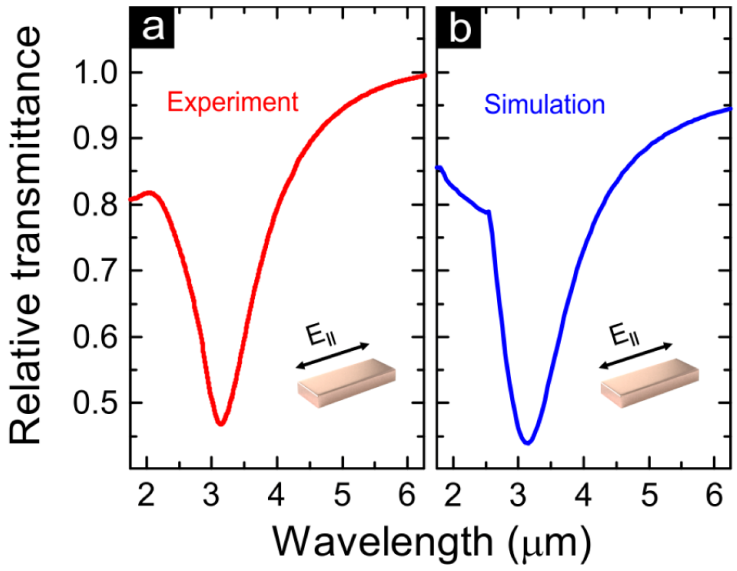

Fig. 3. Simulated (a) and experimental (b) results of relative transmittance spectra of the 50 nm thick TiN antenna arrays fabricated by direct laser writing (parallel polarization, $E_{||}$). The antenna lengths and widths are 0.83 μm and 200 nm, respectively, and the periodicity of antennas parallel to the antenna long (short) axis is 1.5 μm.

A crucial point for applications is the stability of our TiN nanoantenna arrays at high temperatures. As has been shown previously, TiN is a refractory material with excellent thermal stability, even for temperatures above 2000°C [18]. However, high-temperature annealing of TiN in oxygen-containing environment will lead to oxidation of the material [32] and consequently, due to the small size and high surface area of our nanoantennas, cause the complete disappearance of the plasmon resonance in our geometry as shown in Fig. 4(a). Previous studies have shown that TiN will not significantly oxidize at temperatures below 300-350°C [33,34], but as with many nitrides, at higher temperatures such as those explored here, oxidation can become an issue. Whereas annealing of TiN under vacuum condition can prevent oxidization of TiN nanostructures and keep the optical properties of TiN film stable [20], the use of thin dielectric coatings has also been suggested to reduce this oxidation in TiN films [32]. Figure 4(a) shows relative transmittance of the nanoantenna arrays before (blue line) and after annealing (red line) at 800°C. The plasmon resonance clearly disappears after the annealing process. To overcome this problem, we incorporate a 200 nm thick aluminum oxide (Al_2O_3) layer, a refractory dielectric transparent over the near- to mid-IR range, which is sputtered on top of the fabricated TiN nanoantenna arrays in an attempt to prevent oxygen from the surrounding environment from reaching the TiN antennas. The addition of this film only causes a 0.5 μm spectral shift of the antenna resonance to longer wavelengths combined with a slight broadening of the lineshape, while the modulation depth is maintained as shown in Fig. 4(b).

#246613 Received 23 Jul 2015; revised 20 Sep 2015; accepted 14 Oct 2015; published 22 Oct 2015

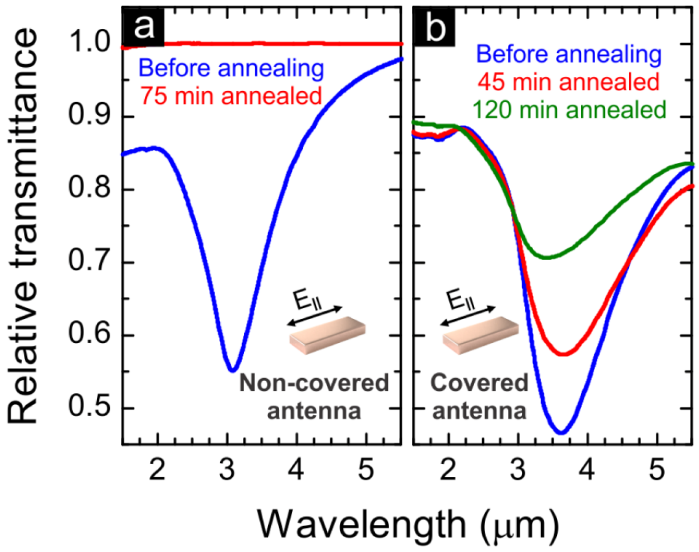

Fig. 4. High-temperature stability of 50 nm thick TiN nanoantenna on sapphire substrate without protection layer as well as covered with 200 nm thick aluminum oxide (Al_2O_3). (a) The TiN nanoantennas (fabricated by direct laser writing) show a pronounced plasmonic resonance at a wavelength of around 3 μm (blue line). After annealing at 800°C the plasmon resonance vanishes due to the oxidization (red line). (b) When the sample is covered with a 200 nm thick Al_2O_3 protective layer, the resonance undergoes a spectral shift of around 0.5 μm to longer wavelengths combined with a slight broadening of the lineshape (blue line). Annealing at a temperature of 800°C induces only a small decrease of the modulation depth of the resonance (red line). Further annealing (green line) causes a degradation of the Al_2O_3 layer and consequently a blue shift of the plasmon resonance as well as a further decrease of the modulation depth (TiN antenna periodicity = 1.5 μm, length = 1.0 μm, width = 200 nm, height = 50 nm).

The sample is then annealed in Ar flow at a temperature of 800°C for about 45 minutes. The argon flow does not prevent oxidization of TiN but is necessary for an accurate measurement of the annealing temperature. Looking again at the optical response of the antenna arrays, we find that the resonance position is maintained while the modulation depth of the resonance decreases by around 15% as shown in Fig. 4 (red line). The reduced modulation depth is most likely due to intrinsic oxygen interdiffusion between Al_2O_3 and TiN or diffusion of oxygen from the native surface oxide (TiO_2) into the thin film. Choosing different oxidization-resistant cap layers, e.g. Si_3N_4, may decrease the rate of oxidization or avoid it entirely. Still, our experiments clearly demonstrate the thermal stability of our Al_2O_3-protected TiN nanoantenna arrays, as confirmed by the pronounced plasmonic resonance visible after annealing.

Our fabrication method enables the fabrication of a wide range of antenna arrays with varying lengths from 0.2 to 1.4 μm. This is demonstrated by displaying selected scanning electron microscope (SEM) images of our nanoantenna arrays on Si substrate. Typical relative transmittance spectra (parallel polarization, $E_{||}$) of the corresponding nanoantenna arrays are shown in Fig. 5(a), demonstrating tunability of the resonance wavelength from the near- to mid-infrared spectral range. The results are in fair agreement with the simulation. The plasmon resonance positions of different nanoantenna arrays fabricated by femtosecond direct laser writing lithography show a clear linear correlation with the antenna lengths as shown in Fig. 5(b). The peak positions correspond to different temperatures of blackbody radiation and can thus be designed to provide the best match with the blackbody emission spectrum for a given temperature [35].

#246613 Received 23 Jul 2015; revised 20 Sep 2015; accepted 14 Oct 2015; published 22 Oct 2015

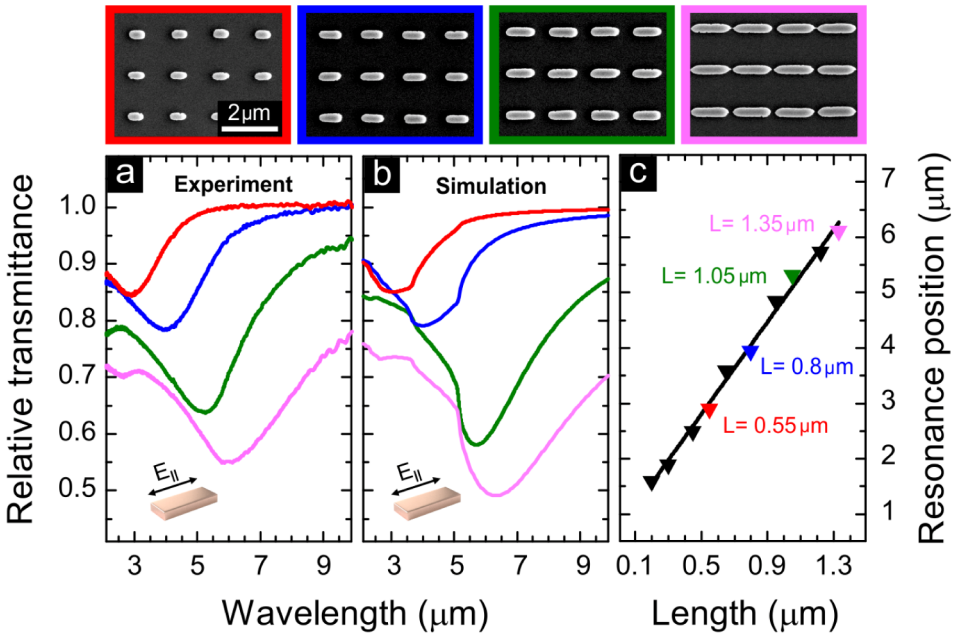

Fig. 5. SEM images, relative transmittance spectra (experiment and simulation), and plasmon resonance positions of TiN antennas fabricated by direct laser writing lithography on a Si substrate are shown. (a) Relative transmittance spectra (parallel polarization, $E_{||}$) of the selected antenna arrays show tunability of the plasmon resonances from the near- to mid-infrared. (b) The corresponding simulated spectra are in fair agreement with experiment. Deviations are due to the imperfect surface of the antennas created by the wet etching process. (c) The plasmon resonance position of the antenna arrays exhibits a linear dependence of the resonance wavelength on the antenna length. Selected antennas are labeled with the corresponding color from panel (a). The periodicity of antennas parallel to both the long and the short antenna axes is 1.5 μm, antenna lengths are varied from 0.2 to 1.35 μm, and the antenna widths and heights are 250 and 50 nm, respectively.

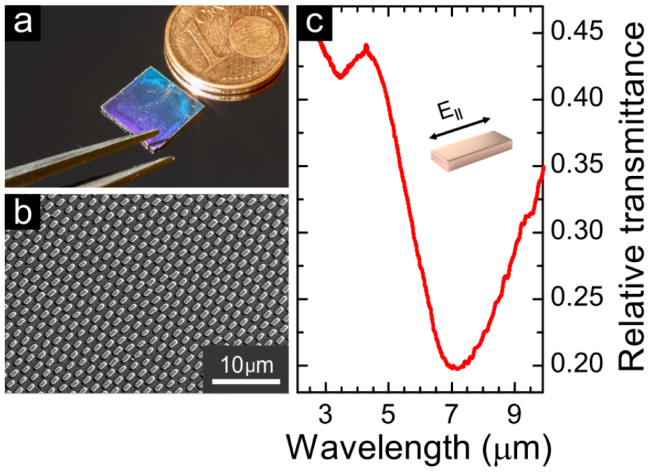

Fig. 6. Large-area fabrication of TiN antennas by laser interference lithography on a Si substrate. (a) A photograph of the sample demonstrates the homogeneity of our antenna arrays over a large area (10 × 10 mm^2). (b) Tilted view scanning electron micrograph of the fabricated TiN antennas (length: 1.7 μm, width: 0.8 μm, height: 50 nm). (c) Relative transmittance spectrum (parallel polarization, $E_{||}$) of the fabricated antennas.

#246613 Received 23 Jul 2015; revised 20 Sep 2015; accepted 14 Oct 2015; published 22 Oct 2015

Direct laser writing lithography can easily provide antenna masks over 200 × 200 μm^2 areas with processing times on the order of a few seconds; however, our approach for nanoantenna fabrication can also easily be extended to other lithographic tools. Particularly, large-area and low-cost fabrication is highly sought after for real-world applications. As an established technique for wafer-scale processing, laser interference lithography is a prime candidate for fabricating large-area plasmonic structures. We demonstrate this by fabricating a large-area sample (10 × 10 mm^2) covered with TiN nanoantennas as shown by the macro photograph in Fig. 6(a). Figure 6(b) shows the typical SEM image of TiN antenna arrays fabricated by interference lithography (periodicity: 2.1 μm, length: 1.7 μm, width: 0.8 μm, height: 50 nm) and demonstrates the excellent homogeneity of our large-area sample. The relative transmittance spectrum of such antenna arrays (parallel polarization, $E_{\parallel}$) clearly shows a plasmon resonance in the mid-infrared (around 7 μm) as evident from Fig. 6(c).

4. Conclusion

We employed direct laser writing as well as laser interference lithography to fabricate TiN nanoantennas with high quality plasmon resonances in the near- and mid-infrared spectral range. Large-area and low-cost preparation of such nanoantenna arrays combined with the intrinsic character of TiN as a refractory material makes such nanoantennas well-suited for high-temperature plasmonic application such as thermophotovoltaics, thermal imaging as well as nano-heat transfer systems. A protective layer of 200 nm Al_2O_3 makes the optical response of the antennas much less susceptible to degradation while annealing at 800°C in argon flow. This indicates that the Al_2O_3 layer improves the thermal stability of our TiN antennas. To prevent oxygen interdiffusion, oxygen-less capping layers such as Si_3N_4 will also be tried in the future. Due to its simplicity and broad applicability, our method opens the door to large-area and low-cost refractory plasmonics in the mid-infrared.

Acknowledgments

The authors gratefully acknowledge financial support by ERC Advanced Grant COMPLEXPLAS as well as DFG, BMBF, GIF, Zeiss foundation, and MWK Baden-Württemberg and the Baden-Württemberg Stiftung. We thank the DFG open access publication fund. The authors also thank Dominik Floess for visualization, Dr. Liwei Fu for FIB cut and taking cross section SEM image and Monika Ubl, Reinhart Völker, and Gabriele Untereiner for technical assistance. TiN films preparation was performed in part at the Center for Nanoscale Systems (CNS), a member of the National Nanotechnology Infrastructure Network (NNIN), which is supported by the National Science Foundation under NSF award no. ECS-0335765. CNS is part of Harvard University.

#246613 Received 23 Jul 2015; revised 20 Sep 2015; accepted 14 Oct 2015; published 22 Oct 2015